CCFE-PR(17)74

L. Garzotti, E. Barbato, J. Garcia, N. Hayashi, G.Giruzzi, P. Maget, M. Romanelli,
S. Saarelma, R. Stankiewitz, M. Yoshida, I. Voitsekhovitch, R. Zagórski

Analysis of JT-60SA operational scenarios

Analysis of JT-60SA operational scenarios

L. Garzotti[1], E. Barbato[2], J. Garcia[3], N. Hayashi[4], G. Giruzzi[3], P. Maget[3], M. Romanelli[1], S. Saarelma[1], R. Stankiewitz[5], M. Yoshida[4], I. Voitsekhovitch[1], R. Zagórski[5]

[1] CCFE, Culham Science Centre, OX14 3DB Abingdon, Oxfordshire, OX14 3DB, United Kingdom
[2] ENEA, C. R. Frascati, Rome, Italy
[3] CEA, IRFM, F-13108 Saint-Paul-lez-Durance, France
[4] National Institutes for Quantum and Radiological Science and Technology, Naka, Ibaraki, 311-0193, Japan
[5] IPPLM, Warsaw, Poland

Analysis of JT-60SA operational scenarios

L. Garzotti†, E. Barbato‡, J. Garcia§, N. Hayashi ‖, G. Giruzzi§, P. Maget§, M. Romanelli†, S. Saarelma†, R. Stankiewitz¶, M. Yoshida ‖, I. Voitsekhovitch†, R. Zagórski¶

† CCFE, Culham Science Centre, OX14 3DB Abingdon, Oxfordshire, OX14 3DB,United Kingdom

‡ ENEA, C. R. Frascati, Rome, Italy

§ CEA, IRFM, F-13108 Saint-Paul-lez-Durance, France

‖ National Institutes for Quantum and Radiological Science and Technology, Naka, Ibaraki, 311-0193, Japan

¶ IPPLM, Warsaw, Poland

Abstract. Reference scenarios for the JT-60SA tokamak have been simulated with one-dimensional transport codes to assess the stationary state of the flat-top phase and provide a profile database for further physics studies (e.g. MHD stability, gyrokinetic analysis) and diagnostics design. The types of scenario considered vary from pulsed standard H-mode to advanced non-inductive steady-state plasmas. In this paper we present the results obtained with the ASTRA, JINTRAC, CRONOS and TOPICS codes equipped with the Bohm/gyro-Bohm, CDBM and GLF23 transport models. The scenario analysed here are a standard ELMy H-mode, a hybrid scenario and a non-inductive steady state plasma with operational parameters from the JT-60SA research plan.

Several simulations of the scenarios under consideration have been performed with the above mentioned codes and transport models. The results from the different codes are in broad agreement and the main plasma parameters generally agree well with the zero dimensional estimates reported previously. The sensitivity of the results to different transport models and, in some cases, to the ELM/pedestal model has been investigated.

PACS numbers: 52.55.Fa, 52.55.Dy, 52.65.-y, 52.25.Fi

1. Introduction

JT-60SA is a tokamak presently under construction in Naka, Japan, using the infrastructure of the existing JT-60 Upgrade experiment. The construction of JT-60SA is a collaboration between Europe and Japan under the broader approach satellite tokamak programme. JT-60SA is designed to support ITER operations and to investigate how to optimise scenarios for future demonstration fusion power plants, which will be built after ITER. The acronym SA stands for 'Super' and 'Advanced', since the experiment will have superconducting coils and study advanced modes of plasma operation. Further details of its experimental programme are explained in the JT-60SA research plan [1].

The intrinsic flexibility of JT-60SA will allow the study of a variety of scenarios. In particular, the scenarios under consideration for plasma operations on JT-60SA are: pulsed, inductive standard H-modes, similar to the ITER baseline scenario; advanced inductive, high-β, low magnetic shear scenarios, similar to the ITER hybrid scenario and fully non-inductive, steady-state, advanced scenarios, which could be extrapolated to a steady-state demonstration fusion power plant. The main parameters of the reference scenarios are given in table 2-3 of reference [1].

The scenarios described above have been developed with the help of the 2-dimensional equilibrium code ACCOME [2] (consistently with current drives) and then assessed by the 0.5-dimensional code METIS [3]. The results have been extensively reported in [4]. To increase the confidence in these simulations and to further check whether the plasma parameters calculated by ACCOME and METIS are achievable, we have modelled the flat top of the baseline, hybrid and fully non-inductive scenario with more sophisticated 1.5-dimensional transport codes. The aim of this paper, which builds on the model validation performed using selected sets of JT-60U and JET discharges [5], is to report the results of these simulations.

The structure of the paper is the following: in section 2 we give a general description of the codes and the transport models deployed in this study and of the simulation condition; in section 3 we describe the results for the baseline H-mode scenario; in section 4 we present the results for the hybrid scenario; in section 5 we describe the results for the advanced steady-state scenario; in section 6 we discuss the results obtained and in section 7 we summarize the main conclusions of the study.

2. Description of the simulations

The transport codes used in the simulations presented in this study were: ASTRA [6], CRONOS [7], JINTRAC [8] and TOPICS [9]. Each transport code is equipped with a number of core transport models. In particular, for the analysis presented in this paper, we used: the physics based transport models GLF23 [10] (implemented in ASTRA, CRONOS and TOPICS) and CDBM [11] (implemented in CRONOS, JINTRAC and TOPICS) and the semi-empirical transport model Bohm/gyro-Bohm [12] (implemented

in ASTRA and JINTRAC).

In all simulations we solve transport equations for the current density and the ion and electron temperature. In CRONOS and JINTRAC the equation for the ion density is also solved and the electron density is obtained from prescribed Z_{eff} profiles and impurity mix, whereas in ASTRA and TOPICS the electron density profiles are prescribed and taken from the ACCOME reference result. Modelling of plasma rotation was included only in the JINTRAC simulations for the advanced steady-state scenario to compare the prediction of different models for the formation of an internal transport barrier (ITB).

Simulating an H-mode plasma requires a model to describe the edge transport barrier (ETB), where the physics governing the transport is much less understood than in the core and the transport is intermittent due to the presence of ELMs. The codes used in this study adopt different approximations to treat this problem. In ASTRA and TOPICS the problem is avoided by imposing the boundary conditions at the top of the ETB and not solving the transport equations inside it, whereas in CRONOS and JINTRAC simulations the boundary conditions are imposed at the separatrix. In particular, in TOPICS, the electron and ion temperature profiles in the pedestal are determined on the basis of a EPED1 pedestal width scaling and a stability check by the linear MHD code MARG2D [13].

In JINTRAC the transport in the ETB can be determined in two ways. The first is to adopt the continuous ELM model described in [14], which mimics the limiting effect of the ELMs on the pressure gradient in the ETB by introducing additional transport averaged over time and clamps the normalized pressure gradient in the ETB α at a prescribed critical value α_c. The second is to directly prescribe the particle diffusivity D and the ion and electron thermal conductivity $\chi_{i,e}$ in the pedestal to obtain the desired density and temperature pedestal height. In both cases the width of the pedestal is prescribed as a free input parameter.

In CRONOS the pedestal energy content is estimated by means of the Cordey two-term scaling [15], the height of the density and temperature pedestal is then calculated by imposing neoclassical transport in the ETB, whereas the pedestal width is obtained from the EPED1 model and turns out to be proportional to $\sqrt{\beta_p}$ [16].

The particle source due to the gas puff and the ionization of the neutral atoms recycling at the wall is described in JINTRAC by FRANTIC [17], where a ray tracing technique is used to calculate the neutral density inside the plasma in cylindrical geometry taking into account ionization and multiple charge exchange processes to determine the profile of the ionization particle source. In CRONOS a Gaussian profile was assumed for the ionization source, the shape of which was tuned against JET and JT-60U data and kept the same in JT-60SA extrapolations [5].

For the simulations presented in this paper, the power deposition associated with additional heating was calculated in CRONOS by means of the codes NEMO/SPOT [18] for the positive and negative neutral beam injection (NBI) heating and REMA [19] for the electron cyclotron resonance heating (ECRH). The same heat source profiles

were then used in ASTRA. In JINTRAC the NBI power deposition was modelled by PENCIL [20], whereas the ECRH power deposition was assumed equal to the one used in the CRONOS and ASTRA simulations. As a consequence, in ASTRA and JINTRAC, the heat deposition profiles are not completely consistent with the final equilibrium density and temperature profiles. In TOPICS, the NBI power deposition heating is calculated with a Fokker Planck model [21] and the NBI-driven current is calculated using Mikkelsen and Singer's approximation [22]. The EC heating and current drive are computed with the EC code described in [23].

The 2-dimensional equilibria for the transport simulations are provided by different equilibrium codes. ASTRA can use either SPIDER [24] or a three-moment representation of the equilibrium, CRONOS uses HELENA [25] as its standard equilibrium solver, JINTRAC calculates the equilibrium with the ESCO solver [26] and TOPICS uses the free-boundary equilibrium code described in [27].

In the study presented in the following section we took as initial condition for the transport simulations the profiles obtained from METIS runs [3] and we run ASTRA, CRONOS and JINTRAC for several confinement times ($\sim$ 10 s) in order to reach equilibrium. TOPICS simulations were run in a similar way but starting from ACCOME results as initial condition. We then compared the 0-dimensional parameter derived from the 1.5-dimensional transport runs and the radial density, temperature and q profiles with the reference parameters and between the different codes. This allowed us to assess the consistency of the reference parameters and of the METIS/ACCOME analysis with more sophisticated transport models and the robustness of the result with respect to the variation of the profiles due to the use of different transport models.

3. Baseline H-mode scenario

The first scenario analysed is a standard H-mode similar to the ITER baseline scenario (referred to as scenario 2 in the JT-60SA research plan). For this scenario $B_T = 2.25$ T, $I_p = 5.5$ MA, $P_{NBI} \approx 34$ MW (10 MW negative NBI and 24 MW positive NBI) and $P_{ECRH} = 7$ MW. The plasma boundary used in the simulations is shown in figure 1.

The boundary conditions on the density and temperature profiles for the simulations of scenario 2 were chosen to match as close as possible the results of integrated core/SOL simulations with the COREDIV code [28]. It should be noted, however, that, because of the different ways impurities are treated in different codes, it was not possible to match exactly the values obtained by COREDIV. Nevertheless, we found that values of $n_e = 2.3 \cdot 10^{19}$ m^{-3} and $T_e = T_i = 150$ eV at the separatrix imply a sputtering rate of impurities (mainly carbon) from the divertor compatible with the assumption $Z_{eff} = 1.8$.

As described in [5], based on the validation of different transport models on specific JET and JT-60U shots, CRONOS simulations use GLF23 for particle and heat transport respectively, whereas TOPICS simulations are limited to heat transport with GLF23. On the other hand, ASTRA and JINTRAC use the semi-empirical Bohm/gyro-Bohm

transport model, which has been extensively validated on JET.

The equilibrium electron density and electron and ion temperatures profiles obtained with ASTRA, CRONOS, JINTRAC and TOPICS are shown in figure 2. To obtain the same electron density and electron and ion temperature at the top of the pedestal in CRONOS and JINTRAC we prescribed in JINTRAC $D = 0.2$ m^2/s and $\chi_{i,e} = 0.2$ m^2/s inside the ETB. It is worth noting that, in these simulations, the value of α, the normalized pressure gradient inside the pedestal, was ~ 2, which is somehow higher than what is observed, for example, on JET and could be beyond the peeling-ballooning stability boundary. These results highlight the importance of having a reliable prediction for the height and width of the density and temperature pedestal and of checking the assumptions made on the pedestal against ballooning stability criteria.

ASTRA gives results broadly in line with CRONOS and JINTRAC, whereas TOPICS predicts the formation of an ITB at $\rho \approx 0.3$. This is because the prescribed density profile features a fairly steep gradient at $\rho \approx 0.5$, which destabilizes the trapped electron modes (TEMs) and results in large diffusivities at this radial position and ITB-like profiles. TEMs can be stabilized by $E \times B$ flow shear, which in JT-60SA can be significant because of the degree of toroidal rotation control achievable thanks to the large amount and the flexibility of the NBI power available. Since the rotation profiles have not been simulated and tested for this scenario, in order to verify the TOPICS result, TOPICS was also used with the CDBM and Bohm/gyro-Bohm transport models. These models, with no or little effect of the $E \times B$ flow shear, showed less good agreement with the JET/JT-60U than GLF23 [5] and predict smoother profiles with almost the same 0-dimensional parameters.

The 0-dimensional parameters derived from these simulations are summarized in table 1 where the reference values (obtained from ACCOME) from the research plan [1] are also reported for comparison. It can be seen that, despite the differences in the density and temperature profiles predicted by the different codes, in general all codes give values for 0-dimensional quantities close to the reference ones.

4. Hybrid scenario

The second scenario simulated in this study is an advanced inductive scenario similar to the ITER hybrid scenario (referred to as scenario 4.2 in the JT-60SA research plan). For this scenario $B_T = 2.28$ T, $I_p = 3.5$ MA, $P_{NBI} \approx 30$ MW (10 MW negative NBI and 20 MW positive NBI) and $P_{ECRH} = 7$ MW. The plasma boundary used in the simulations is shown in figure 3.

Also in this case we prescribed the boundary conditions on the density and temperature profiles on the basis of integrated core/SOL simulations with the COREDIV code, which indicate that $n_e = 1.4 \cdot 10^{19}$ m^{-3} and $T_e = T_i = 100$ eV at the separatrix lead to a sputtering rate of impurities from the divertor compatible with the assumption $Z_{eff} = 2.1$.

Table 1. Reference 0-dimensional parameter for scenario 2 compared with the values obtained from the 1.5-dimensional transport simulations described in the paper.

Scenario 2	JINTRAC	CRONOS	ASTRA	TOPICS	Reference
B_T [T]	2.25	2.25	2.25	2.25	2.25
I_p [MA]	5.5	5.5	5.5	5.5	5.5
f_{bs} [%]	34	28	35	29	28
f_{ni} [%]	46	39	51	51	50
q_{95}	3.5	3.0	3.3	3.1	3.0
P_{NBI} [MW]	33.0	33.0	32.5	34.0	34.0
P_{ECRH} [MW]	7.0	7.0	7.0	7.0	7.0
n_{e0} [10^{19} m^{-3}]	8.2	7.5	8.2	7.7	7.7
$< n_e >$ [10^{19} m^{-3}]	5.1	6.2	5.4	5.6	5.6
T_{e0} [keV]	10.3	8.1	11.2	11.1	13.5
$< T_e >$ [keV]	7.2	5.4	7.0	5.8	6.3
T_{i0} [keV]	12.4	8.5	11.2	12.3	13.5
$< T_i >$ [keV]	6.5	5.8	6.4	6.3	6.3
W_{th} [MJ]	23.0	22.5	23.3	21.2	22.0
β_N []	3.1	3.0	3.1	2.9	3.1
τ_E [s]	0.60	0.61	0.58	0.52	0.64
Z_{eff}	1.8	1.8	1.5	2.0	-

Fully predictive JINTRAC simulations for scenario 4.2 were performed with the Bohm/gyro-Bohm transport model assuming a value for $\alpha_c = 1.5$ in the ETB.

Semi-predictive ASTRA simulations (i. e. simulations where we solved the equations for the ion and electron temperature profiles whereas the density profile was prescribed) were performed for this scenario with the semi empirical Bohm/gyro-Bohm and the physics based GLF23 transport models.

Finally, fully predictive CRONOS simulations similar to scenario 2 were performed with the GLF23 transport model for the density equation and the CDBM transport model for the ion and electron temperature equations.

As for scenario 2, the 0-dimensional parameters derived from these simulations are summarized in table 2 where the values from the research plan are also reported for comparison. It can be seen that, despite the even greater differences in the density and temperature profiles with respect to scenario 2 predicted by the different codes, also in this case in general all codes give values for 0-dimensional quantities close to the reference ones.

The equilibrium electron density and electron and ion temperatures profiles obtained with ASTRA, CRONOS and JINTRAC are plotted in figure 4 and deserve some comments.

First of all, we note that all codes and transport models predict or assume similar

Table 2. Reference 0-dimensional parameter for scenario 4.2 compared with the values obtained from the 1.5-dimensional transport simulations described in the paper.

Scenario 4-2	JINTRAC	CRONOS	ASTRA BgB / GLF23	Reference
B_T [T]	2.28	2.28	2.28 / 2.28	2.28
I_p [MA]	3.5	3.5	3.5 / 3.5	3.5
f_{bs} [%]	48	40	51 / 43	40
f_{ni} [%]	77	66	79 / 75	58
q_{95}	4.6	4.6	4.8 / 4.8	4.4
P_{NBI} [MW]	29	29	29 / 32	30
P_{ECRH} [MW]	6.8	7.0	7.0 / 7.0	7.0
n_{e0} [10^{19} m^{-3}]	6.4	8 6	7.9 / 7.9	8.4
$< n_e >$ [10^{19} m^{-3}]	4.7	5.0	5.0 / 5.0	6.2
T_{e0} [keV]	9.7	8.2	7.8 / 10.0	7.5
$< T_e >$ [keV]	5.2	3.8	4.0 / 3.6	3.7
T_{i0} [keV]	11.3	9.0	8.7 / 13.0	7.5
$< T_i >$ [keV]	4.6	4.3	4.1 / 4.3	3.7
W_{th} [MJ]	14.2	12.5	12.6 / 13.4	13.4
β_N	3.4	3.2	3.0 / 3.2	3.0
τ_E [s]	0.40	0.40	0.35 / 0.40	0.42
Z_{eff}	2.1	2.1	1.7	-

values for the height and width of the density and temperature pedestal, with the exception of ASTRA with the Bohm/gyro-Bohm transport model, where the electron temperature at the top of the ETB does not evolve and is fixed at the beginning of the simulation at a value $\sim$ 30% lower than the one attained by the other codes, and JINTRAC with the Bohm/gyro-Bohm transport model which predicts an ion temperature at the top of the ETB $\sim$ 30% lower than the other codes.

Secondly, we can see that JINTRAC equipped with the Bohm/gyro-Bohm transport model predicts a density profile significantly less peaked than CRONOS with GLF23.

Thirdly, we should note that the rather sharp peak on the electron and ion temperature profile inside $\rho = 0.1$ predicted by ASTRA with GLF23 is due to the fact that this model tends to predict no instabilities near the plasma axis and therefore almost no transport in this region. This is probably unphysical and the electron and ion temperature profiles are expected to be flatter near the magnetic axis because of some residual transport not accounted for by GLF23.

Finally, we can observe the presence of an ITB on the electron and ion temperature profiles predicted by the CRONOS with the CDBM transport model. This is due to the tendency of CDBM to suppress the heat conductivity and develop ITBs in regions of the plasma with low shear and strong pressure gradients.

5. Steady-state scenario

The third scenario simulated is an advanced steady-state scenario (referred to as scenario 5.1 in the research plan). This scenario is based on the results of experiments performed on JET and JT-60U aiming at establishing plasmas with an ITB driving a significant fraction of the bootstrap current. A description of the main characteristics and of the modelling of these experiments can be found in [29] and references within.

In this study we analysed two versions of this scenario. A 'high power' version with $B_T = 1.72$ T, $I_p = 2.3$ MA, $P_{NBI} \approx 30$ MW (10 MW negative NBI and 20 MW positive NBI) and $P_{ECRH} = 7$ MW and a 'low power' version, more conservative from the point of view of MHD stability, with $B_T = 1.72$ T, $I_p = 2.3$ MA, $P_{NBI} \approx 17$ MW (5 MW negative NBI and 12 MW positive NBI) and $P_{ECRH} = 7$ MW. The plasma boundary used in the simulations is shown in figure 5.

Once again, we prescribed the boundary conditions on the density and temperature profiles for the simulations on the basis of integrated core/SOL simulations with the COREDIV code, which indicate that $n_e = 1.3 \cdot 10^{19}$ m^{-3} and $T_e = T_i = 50$ eV at the separatrix lead to a sputtering rate of impurities from the divertor compatible with the assumption $Z_{eff} = 2.0$. It is worth noting that in these JINTRAC simulations the boundary condition on the current density profile was imposed not by prescribing the total plasma current, as in the simulations for the standard H-mode and advanced inductive scenarios, but by prescribing a value of the loop voltage of a few mV (typically in the range between 1 and 2 mV).

Two important points make this scenario particularly difficult to simulate: the sensitivity of the q profile to the non-inductive current drive and the possible formation of an ITB, which in turn could generate a significant amount of bootstrap current. We have investigated these questions in both the 'high power' and 'low power' versions of the scenario and the results are reported in subsection 5.1 and 5.2 respectively.

5.1. Steady-state H-mode scenario: 'high power' version

For the analysis of the 'high power' version of the scenario we performed three JINTRAC runs where we prescribed D and $\chi_{i,e}$ in the ETB to obtain width and height of the density and temperature pedestal similar to those calculated by CRONOS and corresponding to $\alpha_c \sim 1.5$. It should be noted that this value for α_c is lower than the typical values observed, for example, on JET. However, higher α_c values resulted in steeper pressure gradients in the pedestal and in a contribution of the bootstrap current leading to a total plasma current greater than 2.3 MA for the prescribed loop voltage.

The first two simulations used the Bohm/gyro-Bohm transport model complemented with the assumption $\chi_\phi = \chi_i$ for the momentum transport (equivalent to the assumption that the Prandtl number Pr is equal to one across the whole plasma) and and a criterion for the formation of an ITB, which takes into account the magnetic shear s and the ratio $\omega_{E\times B}/\gamma_{ITG}$ between the shear of the $E \times B$ velocity and the growth rate of the ITG modes. In particular, it has been shown in [30] on a statistical basis that

an ITB is formed when the condition $z = -0.14 + s - 1.47\omega_{E\times B}/\gamma_{ITG} < 0$ is satisfied. Therefore, the Bohm term in the expression for D and $\chi_{i,e}$ in the mixed Bohm/gyro-Bohm transport model is multiplied by $\Theta(z)$, where Θ is the Heaviside step function. It is worth noting that the expression used in JINTRAC for γ_{ITG} has the simplified form $\gamma_{ITG} = v_{th,i}/L_T$, where $v_{th,i}$ is the ion thermal velocity and $L_T = \nabla T/T$.

In one simulation, the power deposition, current drive and torque profile associated with the beam injection were prescribed accordingly to the NEMO/SPOT calculation for a CRONOS simulation of the same scenario (and, as a consequence, were not self-consistent with the density and temperature profiles predicted by JINTRAC), whereas in the other they were calculated self-consistently by PENCIL inside JINTRAC. A Gaussian shape centred at $\rho = 0.4$ for the current density associated with electron cyclotron current drive (ECCD) profile was prescribed in both simulation and the total ECCD-driven current was 150 kA.

The third JINTRAC simulation used the CDBM transport model and the NBI power deposition, current drive and torque profile calculated by PENCIL. In this way we were able to test the sensitivity of the ITB formation to the transport model and of the q profile to the details of the beam power deposition, current drive and torque profile.

The results are summarized in figures 6, 7, 8 and 9. In figure 6, 7, 8 we show the total current density profile, the neutral beam-driven current density and the bootstrap current density for the three cases. Unsurprisingly, the shape of the q profile is very sensitive to the on-axis current density. PENCIL predicts less on-axis current density and a significantly hollow q profile, whereas NEMO/SPOT predicts a higher on-axis density and only a moderately reversed q profile. This might be due to the fact that PENCIL does not take into account the finite size of the fast ion orbits, whereas NEMO/SPOT does and therefore allows for the beam fast ions deposited off-axis to reach the centre of the plasma and contribute to the on-axis current drive.

It is worth noting that the hollow q profiles produced by the markedly off-axis neutral beam-driven current density profile predicted by PENCIL make the calculation of the equilibrium numerically difficult. In fact, the simulations performed using PENCIL could only be extended for 15-20 s and had to be stopped before the current density profile was completely relaxed. However, this time is much longer than the confinement time and therefore the kinetic profiles could relax almost to a complete stationary state.

As for the density and temperature profiles, figure 9 shows that all three JINTRAC runs predict the formation of an ITB at $\rho = 0.45$. The ITB is stronger in the case of the Bohm/gyro-Bohm transport model and weaker in the case of the CDBM transport model. From figure 9, we can also see that these results are in line with the CRONOS simulation using the GLF23 transport model for the density and the CDBM transport model for the ion and electron temperature. In the CRONOS case, the ITB predicted by the CDBM transport model is stronger than the ITB predicted by the same model implemented in JINTRAC. However, the formation of an ITB in CDBM is very sensitive

Table 3. Reference 0-dimensional parameter for scenario 5.1 ('high power' version) compared with the values obtained from the 1.5-dimensional transport simulations described in the paper.

Scenario 5-1	JINTRAC	CRONOS	ASTRA	Reference
B_T [T]	1.72	1.72	1.72	1.72
I_p [MA]	2.4	2.3	2.3	2.3
f_{bs} [%]	62	67	53	68
f_{ni} [%]	100	106	87	100
q_{95}	6.3	6.5	6.6	5.8
P_{NBI} [MW]	29	29	31	30
P_{ECRH} [MW]	6.5	7.0	7.0	7.0
n_{e0} [10^{19} m^{-3}]	6.0	7.0	6.7	.6
$< n_e >$ [10^{19} m^{-3}]	4.2	4.4	4.2	.2
T_{e0} [keV]	5.9	8.0	5.1	6.7
$< T_e >$ [keV]	3.3	3.0	2.8	3.3
T_{i0} [keV]	5.5	8.2	3.9	7.1
$< T_i >$ [keV]	2.9	3.0	2.2	3.4
W_{th} [MJ]	8.9	9.0	7.2	8.4
β_N []	4.8	4.7	3.9	4.3
τ_E [s]	0.24	0.25	0.19	0.31
Z_{eff}	2.0	2.0	2.0	-

to the details of the gradient of the pressure profile and to the local shear. Therefore, small differences in the pressure or the q profile between the two runs can result in significantly different ITBs.

In figure 9, we compare the JINTRAC and CRONOS results with an ASTRA simulation of the same scenario using a three-moment equilibrium and the Bohm/gyro-Bohm transport model, but without any prescription for the formation of an ITB. In this case the absence of an ITB results in a lower energy content and in ion and electron temperature lower than in JINTRAC and CRONOS.

As for the previous scenarios, the 0-dimensional parameters derived from these simulations are summarized in table 3 where the reference values are also reported for comparison. Also in this case it can be seen that, despite the differences in the density and temperature profiles predicted by the different codes, in general all codes give values for 0-dimensional quantities close to the reference. In particular the bootstrap fraction of the total current f_{bs} is between 60% and 70% in all cases predicting the existence of an ITB and it does not depend critically on the strength of th ITB itself. It is interesting to note that even in a case without ITB the ASTRA simulation predicts for this scenario $f_{bs} > 50\%$.

5.2. Steady-state H-mode scenario: 'low power' version

For the analysis of the 'low power' version of scenario 5.1 we performed two JINTRAC runs similar to those executed for the 'high power' version of the scenario.

The first run is a fully predictive simulation where we solved the equations for the current, the density, the ion and electron temperature and the toroidal rotation using the Bohm/gyro-Bohm transport model with the inclusion of an ITB, as described in the previous subsection. The second run was a semi-predictive JINTRAC simulation where we prescribed the same the density profile used in TOPICS and solved the equations for the current and the ion and electron temperature. In this simulation we used the CDBM transport model for heat transport. It should be noted that, in this second simulation, we used the CDBM transport model in the region $\rho \leq 0.8$ and prescribed a fixed value for $\chi_{e,i}$ for $0.8 < \rho \leq 1$ in order to approach at $\rho = 0.8$ the ion and electron temperature that TOPICS obtains by imposing the boundary conditions at $\rho = 0.85$.

In both cases the power deposition, current drive and torque profile associated with the beam were calculated self-consistently by PENCIL inside JINTRAC. The prescription for the current density profile associated with the ECCD was the same as in the 'high power' simulations. In this way we were able to test the sensitivity of the ITB formation to the transport model and of the q profile to the details of the beam power deposition, current drive and torque profile.

The results are summarized in figures 10, 11 and 12. In figure 10 and 11 we show the total current density profile, the neutral beam-driven current density and the bootstrap current density for the two cases. It can be seen that the peak of the bootstrap and the beam-driven current density profile are displaced towards higher ρ for the Bohm/gyro-Bohm simulation with respect to CDBM. This is due to the fact that, although both models predict the formation of an ITB, the Bohm/gyro-Bohm transport model tends to predict a wider barrier than CDBM, as shown in figure 12. Also, the Bohm/gyro-Bohm transport model predicts a wider density profile compared to CDBM, which causes the beam penetration to be more peripheral. The effect of these differences is that, for the applied V_{loop}, in the Bohm/gyro-Bohm case it should be possible to drive almost completely non-inductively the 2.3 MA foreseen for this scenario, whereas the total current obtained in the CDBM case is only ≈ 2.0 MA.

JINTRAC results obtained with the Bohm/gyro-Bohm transport model are in broad agreement with TOPICS results obtained with the CDBM transport model [29] and indicate that scenario 5.1 could achieve a fully non-inductive current of 2.3 MA. This is not the case for JINTRAC simulations with the CDBM transport model, which show that the low power version of scenario 5.1 may not be achieved completely non-inductively. This difference may be caused by the residual difference of pedestal profiles and the lower bootstrap current driven by the ETB. More importantly, it should be noted that one major difference between JINTRAC and TOPICS simulations is that for JINTRAC simulations the total beam-driven current I_{nb} was lower than the one predicted by TOPICS with the CDBM transport model (due to the small contribution

of the EC driven current to the total current in this scenario, I_{nb} can be approximately estimated as $I_{nb} \approx I_p(f_{ni} - f_{bs})$ using for f_{ni} and f_{bs} the values in table 4). These results show that, although the existence of an ITB and its radial position and strength may be important to achieve a low-power version of the fully non-inductive scenario 5.1, an equally important role is played by the beam-driven current and the feasibility of the scenario depends crucially on the NBI driving enough current.

The density and temperature profiles obtained with the different codes and transport models are shown in figure 12. As stated above, JINTRAC predicts the formation of a wider ITB ($\rho \approx 0.45$) with the Bohm/gyro-Bohm model than with the CDBM model ($\rho \approx 0.3$). The result of JINTRAC with the Bohm/gyro-Bohm model is close to the one of TOPICS with CDBM insofar both models predict the formation of an ITB at the same location ($\rho \approx 0.45$). However, JINTRAC gives a suppression of heat conductivity only locally, whereas TOPICS indicates that the heat transport is suppressed to or below the ion neo-classical level inside the ITB. For this reason the two codes give different predictions for on-axis T_e and T_i.

In figure 12 we plot also the result of a CRONOS simulation where the density profile was prescribed as in the TOPICS simulation and the CDBM transport model was used to predict the ion and electron temperature. The resulting temperature profiles are close to the JINTRAC results obtained with the Bohm/gyro-Bohm model.

Finally, it is worth mentioning that the difference in the location of the ITB between the simulation with JINTRAC and CDBM and the simulations with CRONOS and TOPICS with CDBM is due to the different shape of the q profile and the strong sensitivity of the CDBM transport model to it.

As for the previous scenarios, the 0-dimensional parameters derived from these simulations are summarized in table 4. The result indicate that, in general, despite the differences in the density and temperature profiles predicted by the different codes, all codes give values for 0-dimensional quantities close to each other and that even the 'low power' version of scenario 5.1 should achieve a fully non-inductive steady state. In addition, this 'low power' version of scenario 5.1 would operate at a safer level of β_N, in order to avoid MHD instabilities. However, this 'scaled-down' version of the scenario is more sensitive to the details of the beam-driven current density profile. In fact, the total beam-driven current might not be sufficient to achieve fully non-inductive steady-state plasma.

6. Discussion

The simulations described in the previous sections aimed at assessing the sensitivity of the general performance of three of the main operational scenarios envisaged for JT-60SA to the physical assumptions on the core transport model and the behaviour of the pedestal. To this purpose we used different codes equipped with semi-empirical and physics based transport models and making different assumptions on the height and the width of the density and temperature pedestal and compared the results between them

Table 4. 0-dimensional parameter for scenario 5.1 ('low power' version) obtained from the 1.5-dimensional transport simulations described in the paper.

Scenario 5-1	JINTRAC CDBM / BgB	*CRONOS*	TOPICS
B_T [T]	1.72 / 1.72	1.72	1.72
I_p [MA]	2.0 / 2.3	2.3	2.3
f_{bs} [%]	80 / 67	61	72
f_{ni} [%]	94 / 83	83	94
q_{95}	6.6 / 6.5	5.6	5.4
P_{NBI} [MW]	17 / 17	17	17
P_{ECRH} [MW]	7 / 7	7	7
n_{e0} [10^{19} m^{-3}]	7.0 / 5.5	7.0	7.1
$< n_e >$ [10^{19} m^{-3}]	4.1 / 4.2	4.1	4.1
T_{e0} [keV]	5.2 / 5.0	5.6	6.5
$< T_e >$ [keV]	2.7 / 3.3	3.2	3.3
T_{i0} [keV]	5.0 / 4.7	5.9	6.7
$< T_i >$ [keV]	2.5 / 3.0	3.2	3.4
W_{th} [MJ]	6.7 / 8.0	8.0	9.0
β_N []	3.8 / 3.5	3.7	3.9
τ_E [s]	0.28 / 0.38	0.33	0.37
Z_{eff}	2.0 / 2.0	2.0	2.0

and with the reference 0-D values.

The main indication emerging from the set of simulations performed is that, if the properties of the H-mode pedestal are similar, the variability in the main 0-dimensional parameters for each scenario due to the use of different core transport models remains within 30-40% even though the local differences in the density and temperature profiles can be significant (up to 70%). Moreover, the 0-dimensional parameters obtained from the transport simulations described in this paper are in good agreement with the reference values in the research plan and give confidence on the robustness of the scenarios with respect to variations of the details of the radial profiles.

Particular care should be used in the modelling of the advanced steady-state scenario. All codes predict the formation of an ITB, but its strength and location vary from code to code. For the 'high power' version of the scenario, these differences do not influence dramatically the predicted 0-dimensional parameters of the scenario, indicating that such a scenario should be achievable independently of the fine details of the profile of the non-inductively driven current density. However, the 'low power' version of the scenario is more sensitive to the details of the beam-driven current density profile. Indeed, one would expect that with less beam power available the tailoring of the deposition profile becomes comparatively more critical.

Moreover, it is important to note that both from the point of view of predicting the total stored energy and the global plasma performance and from the point of view of assessing the feasibility of a steady-state fully non-inductive plasma scenario it is essential to accurately model the characteristic of the density and temperature pedestal. Unfortunately, this is an area where there are fewer and less reliable models available with respect to the core transport and significant effort will be required to reach a level of reliability of the simulations sufficient to reduce the uncertainty associated with this aspect of the scenario modelling.

Finally, given that one of the missions of JT-60SA will be to explore and prepare scenarios for Demo, it should be pointed out that, although the predictions of the different codes for the general performance of the D-D scenario analysed are similar, the differences may become significant when extrapolating to D-T. Relatively small difference in the predicted T_i profiles, for example, could be amplified and lead to considerably different results in terms of fusion performances and neutron yield. In this sense JT-60SA will play an important role in helping discriminate between different transport models.

7. Conclusions

In this paper we have presented simulations of the flat-top phase of the main JT-60SA operational scenarios performed with different codes and transport models. The results have been compared with the predictions of simpler codes featuring only a simplified description of the transport properties of the plasma.

The results show that, although the details of the kinetic profiles may differ from code to code, within the range of codes employed in the simulations, the results of the one-dimensional simulations are in line with the projected scenarios. The degree of variability between the prediction of the different transport models is within 30% for the most important zero-dimensional plasma parameters. The only caveat comes from the fully non-inductive steady-state scenario. Our simulations indicate that the feasibility of the low-power version of this scenario could depend crucially on the details of the beam-driven current density profile.

Nevertheless, it is important to stress that the above conclusions are true when the codes are tuned against each other to replicate similar density and temperature pedestal characteristics (i. e. width and height). Different assumptions on the pedestal performance could lead to significantly different predictions even when using the same core transport model. Therefore it is important to develop a reliable model capable to predict the behaviour of the density and temperature pedestal and integrated it into the core transport simulations. Such a task, however, is beyond the scope of this paper.

On a shorter time scale, although the pedestal pressure gradients assumed in the simulations for the three scenarios appear to be below the peeling-ballooning stability limit, it would be important to analyse the stability properties of the pedestal profiles with state-of-the-art boundary stability codes. This activity, together with the analysis

of the time dependent phases of the scenarios (i. e. current ramp-up and ramp-down) is planned within the EUROFusion JT-60SA work package.

Finally, it should be noted, however, that more significant differences between predictions obtained with different codes may appear in the extrapolation from the scenarios presented in this paper to D-T plasmas, where the neutron yield will vary more significantly between different simulations, or to a metal divertor, where the accumulation of heavy impurities (not simulated in the present study) will depend critically on the details of the kinetic profiles [31].

Acknowledgments

This work has been carried out within the framework of the EUROfusion Consortium and has received funding from the Euratom research and training programme 2014-2018 under grant agreement No 633053 and from the RCUK Energy Programme [grant number EP/P012450/1]. The views and opinions expressed herein do not necessarily reflect those of the European Commission.

The authors gratefully acknowledge members of the JT-60SA Integrated Project Team for data exchange and fruitful discussions.

References

[1] JT60SA - RP v3.3, http://www.jt60sa.org/pdfs/JT-60SA_Res_Plan.pdf

[2] Tani K, Azumi M and Devoto R S 1992 *J. Comp. Phys.* **98** 332

[3] Artaud J F, Imbeaux F, Aniel T, Basiuk V, Eriksson L G, Giruzzi G, Hoang G T, Huysmans G, Joffrin E, Peysson Y, Schneider M and Thomas P 2005 *32nd European Physical Society Conference on Plasma Physics and Controlled Fusion combined with the 8th International Workshop on Fast Ignition of Fusion Targets (Tarragona, Spain, 26 June - 1 July 2005)* vol **29C** (Europhysics Conference Abstracts) eds Hidalgo C and van Milligen B Ph (Mulhouse: European Physical Society) P1.035

[4] Giruzzi G, Artaud J F, Joffrin E, Garcia J, Ide S, JT-60SA Research Plan Contributors and the JT-60SA Team 2012 *39th European Physical Society Conf. on Plasma Physics and 16th International Congress on Plasma Physics (Stockholm, Sweden, 2 - 6 July 2012)* vol **36F** (Europhysics Conference Abstracts) eds Ratynskaya S, Blomberg L and Fasoli A (Mulhouse: European Physical Society) P5.018

[5] Garcia J, Hayashi N, Baiocchi B, Giruzzi G, Honda M, Ide S, Maget P, Narita E, Schneider M, Urano H, the JT-60U Team, the JET EFDA Contributors and the EU-ITM ITER Scenario Modelling Group 2014 *Nucl. Fusion* **54** 093010

[6] Pereverzev G V and Yushmanov P N 2002 *ASTRA Automated System for TRansport Analysis in a Tokamak*, Max-Planck-Institut fur Plasmaphysik, IPP-Report 5/98

[7] Artaud J F, Basiuk V, Imbeaux I, Schneider M, Garcia J, Giruzzi G, Huynh P, Aniel T, Albajar F, Ané J M, Bécoulet A, Bourdelle C, Casati A, Colas L, Decker J, Dumont R, Eriksson L G, Garbet X, Guirlet R, Hertout P, Hoang G T, Houlberg W, Huysmans G, Joffrin E, Kim S H, Köchl F, Lister J, Litaudon X, Maget P, Masset R, Pégourié B, Peysson Y, Thomas P, Tsitrone E and Turco F 2010 *Nucl. Fusion* **51** 043001

[8] Romanelli M, Corrigan G, Parail V, Wiesen S, Ambrosino R, Da Silva Aresta Belo P, Garzotti L, Harting D, Köchl F, Koskela T, Lauro-Taroni L, Marchetto C, Mattei M, Militello-Asp E, Nave

M F F, Pamela S, Salmi A, Starnd P, Szepesi G and EFDA-JET Contributors 2014 *Plasma and Fusion Research* **9** 3403023

[9] Hayashi N and JT-60 Team 2010 *Phys. Plasmas* **17** 056112

[10] Waltz R E, Staebler G M, Dorland W, Hammett G W, Kotschenreuther K and Konings J A 1997 *Phys. Plasmas* **4** 2482

[11] Itoh K, Itoh S-I, Fukuyama A, Yagi M and Azumi M 1994 *Plasma Phys. Control. Fusion* **36** 279

[12] Erba M, Cherubini A, Parail V V, Springmann E and Taroni A 1997 *Plasma Phys. Control. Fusion* **39** 261

[13] Aiba N, Tokuda S, Ishizawa T, Okamoto M, 2006 *Comput. Phys. Commun.* **175** 269

[14] Parail V, Belo P, Boerner P, Bonnin X, Corrigan G, Coster D, Ferreira J, Foster A, Garzotti L, Hogeweij G M D, Houlberg W, Imbeaux F, Johner J, Köchl F, Kotov V, Lauro-Taroni L, Litaudon X, Lonnroth J, Pereverzev G, Peysson Y, Saibene G, Sartori R, Schneider M, Sips G, Strand P, Tardini G, Valovič M, Wiesen S, Wischmeier M, Zagórski R, JET EFDA contributors and EU ITM Task Force 2009 *Nucl. Fusion* **49** 075030

[15] Cordey J G for the ITPA H-Mode Database Working Group and the ITPA Pedestal Database Working Group 2003 *Nucl. Fusion* **43** 670

[16] Snyder P B, Groebner R J, Hughes J W, Osborne T H, Beurskens M, Leonard A W, Wilson H R and Xu X Q 2011 *Nucl. Fusion* **51** 103016

[17] Tamor S 1981 *J. Comput. Phys.* **40** 104

[18] Schneider M, Eriksson L G, Jenkins I, Artaud J F, Basiuk V, Imbeaux F, Oikawa T, JET-EFDA contributors and ITM-TF contributors 2011 *Nucl. Fusion* **51** 063019

[19] Krivenski V, Fidone I, Giruzzi G, Granata G, Meyer R L and Mazzucato E 1985 *Nucl. Fusion* **25** 127

[20] Challis C D, Cordey J G, Hamnen H, Stubberfield P M, Christiansen J P, Lazzaro E, Muir D G, Stork D and Thompson E 1989 *Nucl. Fusion* **29** 563

[21] Rome J A, McAlees D G, Callen J D, Fowler R H, 1976 *Nucl. Fusion* **16** 55

[22] Mikkelsen D R, Singer C E, 1983 *Nucl. Technol./Fusion* **4** 237

[23] Hamamatsu K, Fukuyama A, 2001 *Fusion Eng. Design* **53** 53

[24] Ivanov A A, Khayrutdinov R R, Medvedev S Yu, Poshekhonov Yu Yu 2005 *32nd European Physical Society Conference on Plasma Physics and Controlled Fusion combined with the 8th International Workshop on Fast Ignition of Fusion Targets (Tarragona, Spain, 26 June - 1 July 2005)* vol **29C** (Europhysics Conference Abstracts) eds Hidalgo C and van Milligen B Ph (Mulhouse: European Physical Society) P5.063

[25] Huysmans G T A, Goedbloed J P and Kerner W 1991 *Computational Physics: Proceedings of the CP90 Europhysics Conference (Amsterdam, The Netherlands, 10 - 13 September 1990)* ed Tenner A (Singapore: Word Scientific) 371

[26] Cenacchi G and Rulli M 1988 *Upgrading of an equilibrium-transport Code for a multispecies free-boundary plasma*, ENEA Report RTI/TIB(88)5

[27] Honda M 2010 *Comp. Phys. Commun.* **181** 1490

[28] Zagórski R, Giruzzi G, Gałazka K, Ivanova-Stanik I, Romanelli M and Stepniewski W 2016 *Nucl. Fusion* **56** 016018

[29] Hayashi N, Garcia J, Honda M, Narita E, Ide S, Giruzzi G, Sakamoto Y, the JT-60U Team, the JET Contributors and JT-60SA Research Unit, *Transport modelling of JT-60U and JET plasmas with internal transport barriers towards prediction of JT-60SA high-beta steady-state scenario*, to be submitted

[30] Tala T J J, Heikkinen J A, Parail V V, Baranov Yu F and Karttunen S J 2001 *Plasma Phys. Control. Fusion* **43** 507

[31] Casson F J, Angioni C, Belli E A, Bilato R, Mantica P, Odstrcil T, Pütterich T, Valisa M, Garzotti L, Giroud C, Hobirk J, Maggi C F, Mlynar J, Reinke M L, JET EFDA Contributors and ASDEX-Upgrade Team 2015 *Plasma Phys. Control. Fusion* **57** 0141031

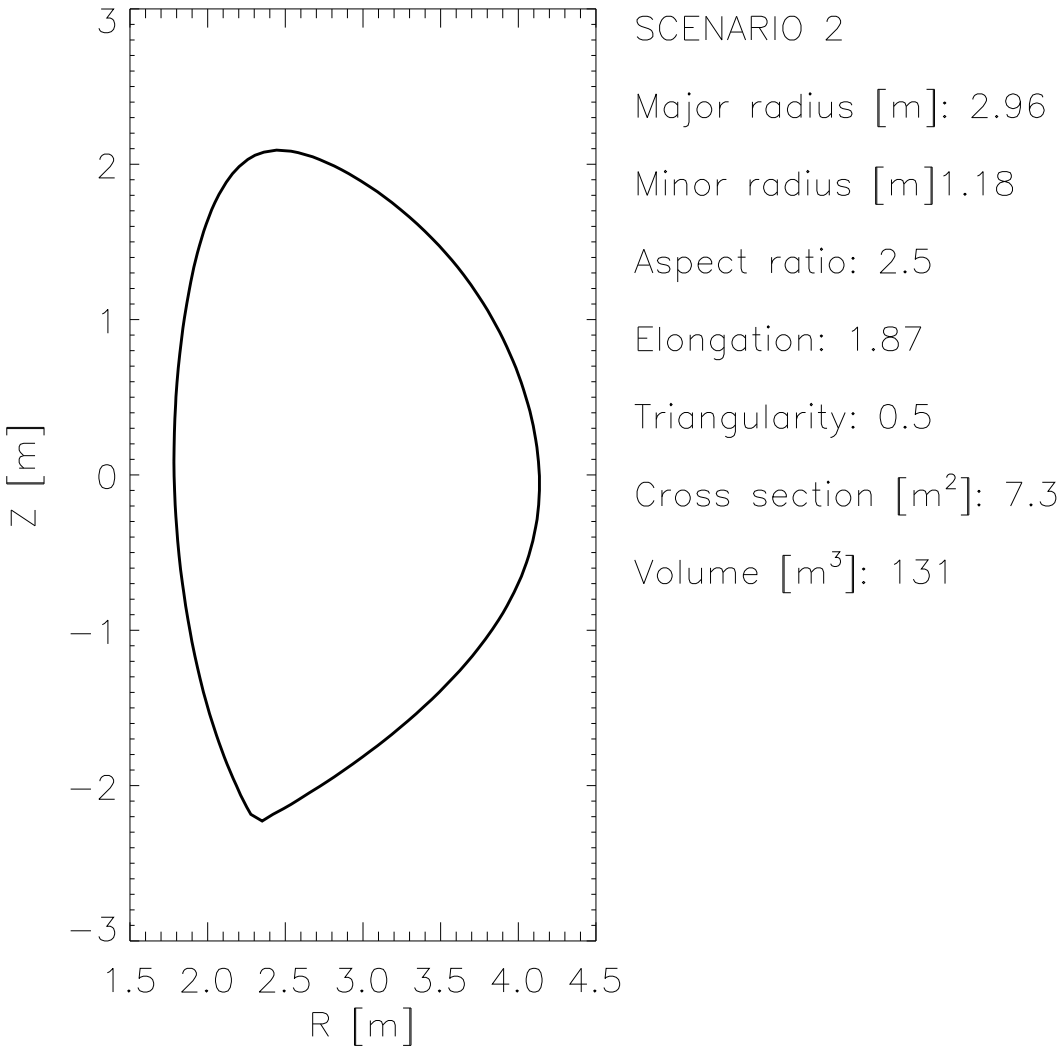

Figure 1. Plasma boundary and main geometrical parameters used in the simulation of a JT-60SA H-mode plasma (scenario 2).

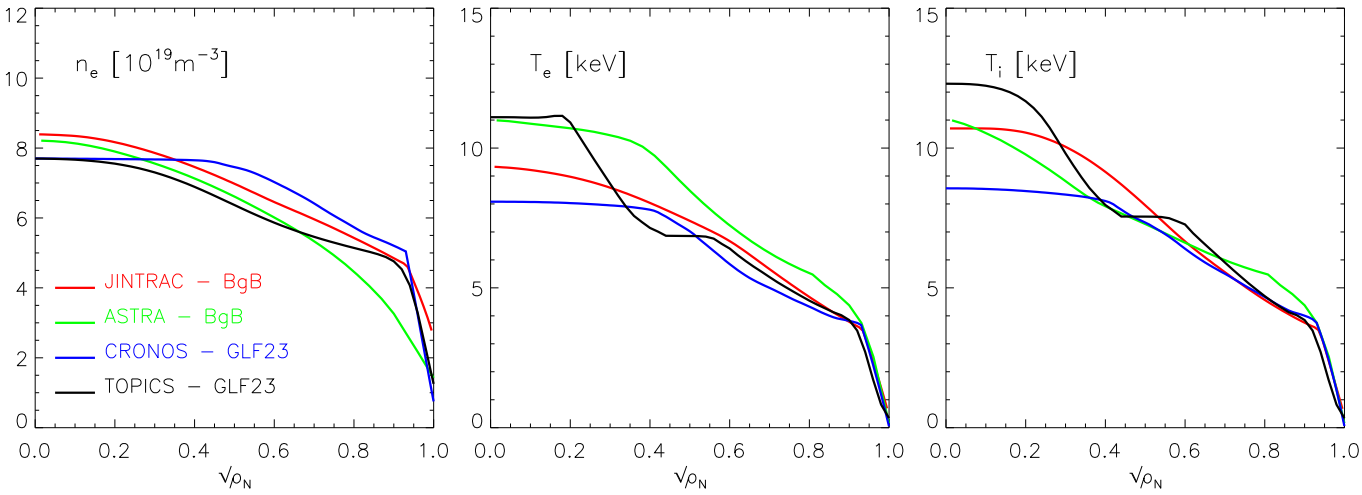

Figure 2. Predicted electron density, electron temperature and ion temperature profiles for a JT-60SA H-mode plasma (scenario 2). The codes and the transport models used in the simulations are indicated in the legend.

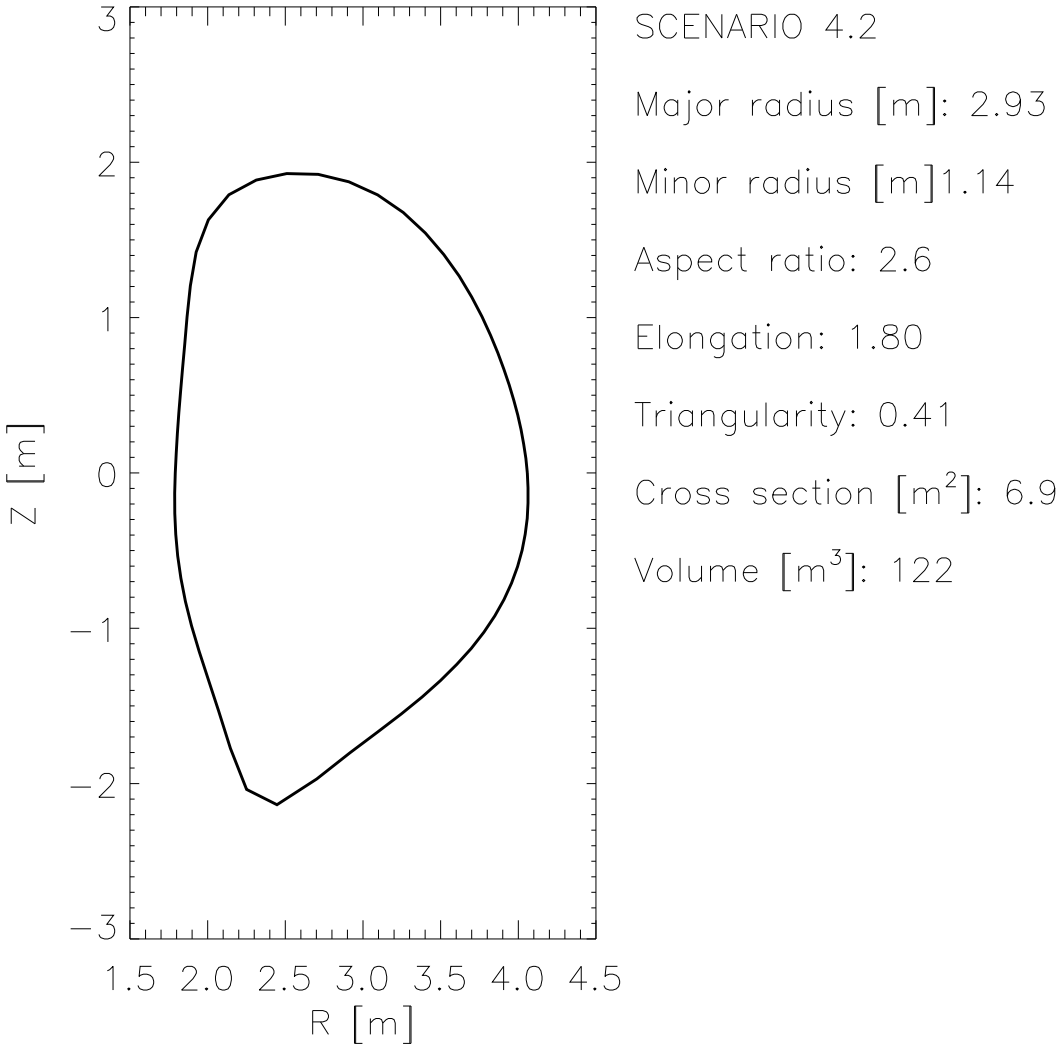

Figure 3. Plasma boundary and main geometrical parameters used in the simulation of a JT-60SA hybrid plasma (scenario 4.2).

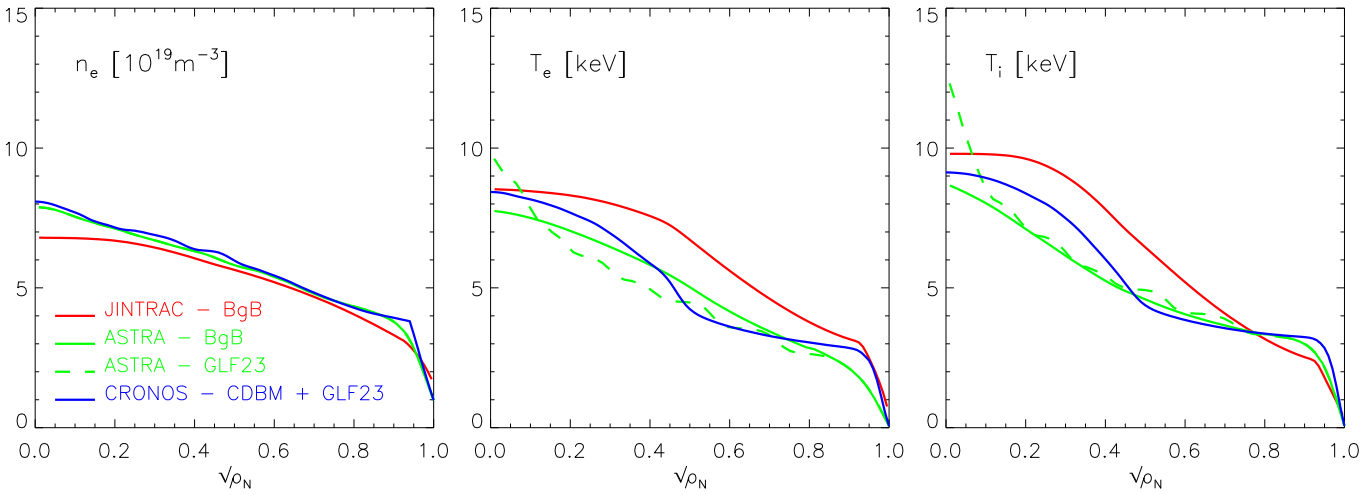

Figure 4. Predicted electron density, electron temperature and ion temperature profiles for a JT-60SA hybrid plasma (scenario 4.2). The codes and the transport models used in the simulations are indicated in the legend.

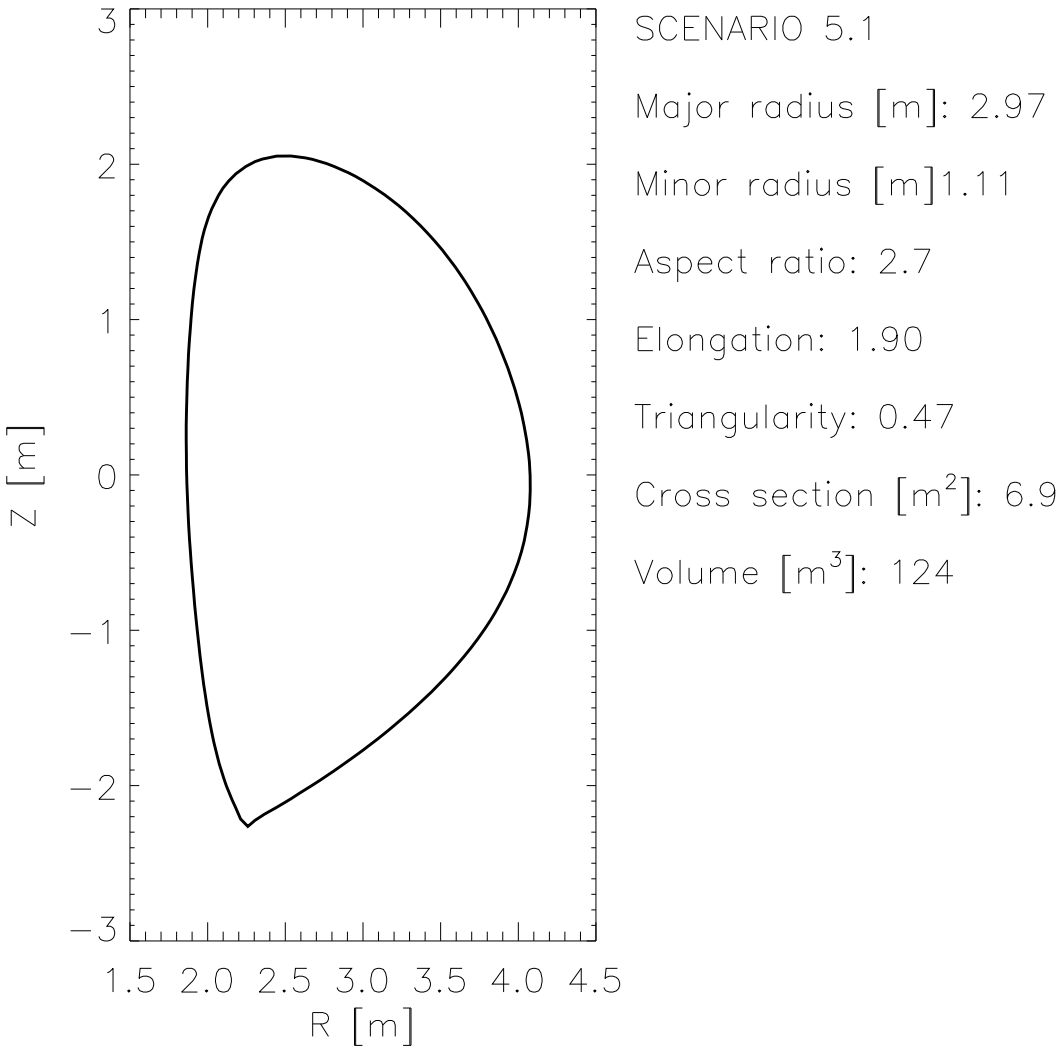

Figure 5. Plasma boundary and main geometrical parameters used in the simulation of a JT-60SA advanced steady-state plasma (scenario 5.1).

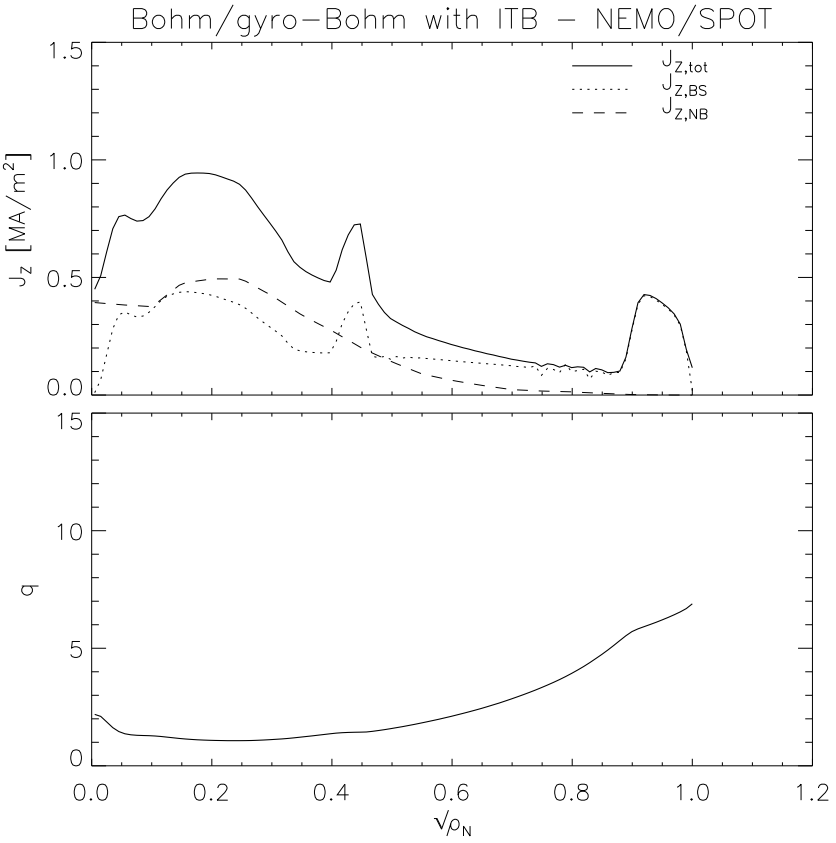

Figure 6. Total current density j_z, neutral beam-driven current density $j_{z,NB}$, bootstrap current density $j_{z,BS}$ and safety factor q profiles for a JT-60SA advanced steady-state plasma (scenario 5.1 'high power' version). The transport model used in the simulation is the Bohm/gyro-Bohm transport model and the neutral beam-driven current density is calculated with NEMO/SPOT (not self-consistently).

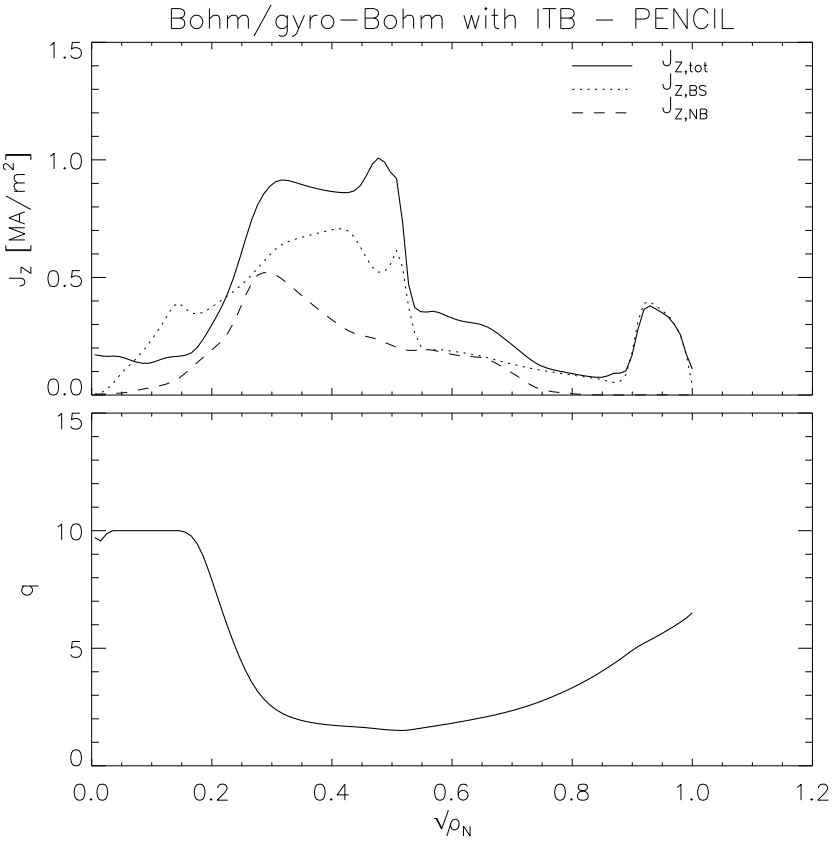

Figure 7. Total current density j_z, neutral beam-driven current density $j_{z,NB}$, bootstrap current density $j_{z,BS}$ and safety factor q profiles for a JT-60SA advanced steady-state plasma (scenario 5.1 'high power' version). The code used in the simulation is JINTRAC with the Bohm/gyro-Bohm transport model and the neutral beam-driven current density is self-consistently calculated with PENCIL.

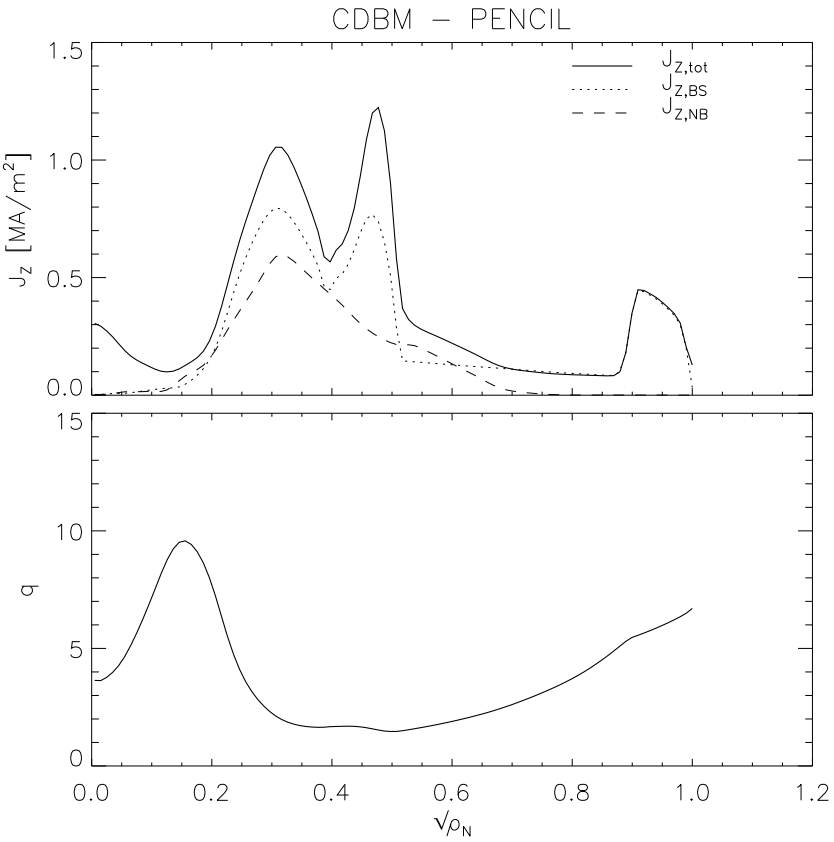

Figure 8. Total current density j_z, neutral beam-driven current density $j_{z,NB}$, bootstrap current density $j_{z,BS}$ and safety factor q profiles for a JT-60SA advanced steady-state plasma (scenario 5.1 'high power' version). The code used in the simulation is JINTRAC with the CDBM transport model and the neutral beam-driven current density is self-consistently calculated with PENCIL.

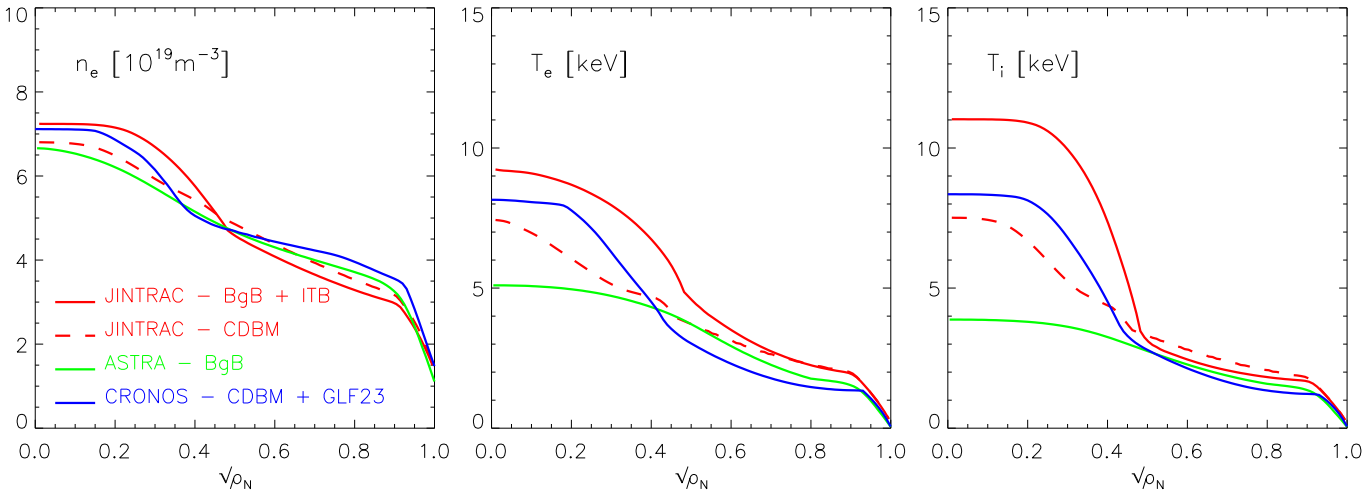

Figure 9. Predicted electron density, electron temperature and ion temperature profiles for a JT-60SA advanced steady-state plasma (scenario 5.1 'high power' version). The codes and the transport models used in the simulations are indicated in the legend.

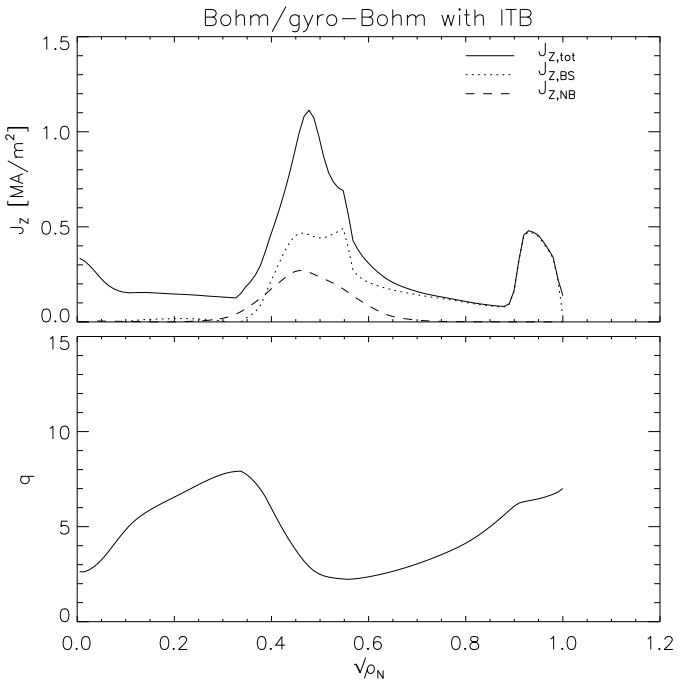

Figure 10. Total current density j_z, neutral beam-driven current density $j_{z,NB}$, bootstrap current density $j_{z,BS}$ and safety factor q profiles for a JT-60SA advanced steady-state plasma (scenario 5.1 'low power' version). The code used in the simulation is JINTRAC with the Bohm/gyro-Bohm transport model and the neutral beam-driven current density is calculated with PENCIL.

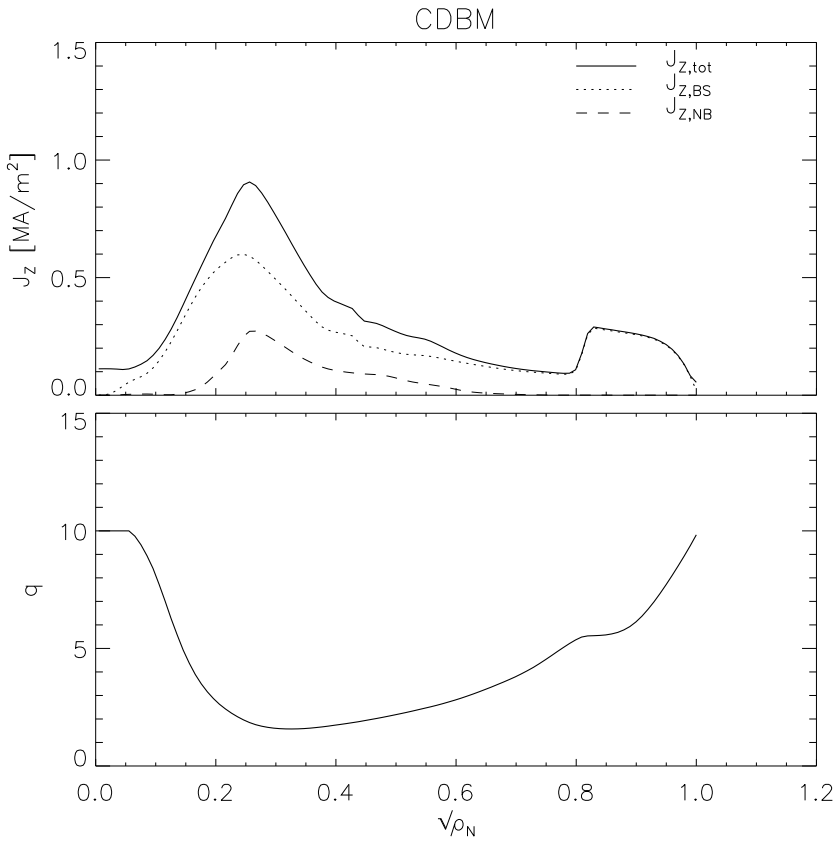

Figure 11. Total current density j_z, neutral beam-driven current density $j_{z,NB}$, bootstrap current density $j_{z,BS}$ and safety factor q profiles for a JT-60SA advanced steady-state plasma (scenario 5.1 'low power' version). The code used in the simulation is JINTRAC with the CDBM transport model and the neutral beam-driven current density is self-consistently calculated with PENCIL.

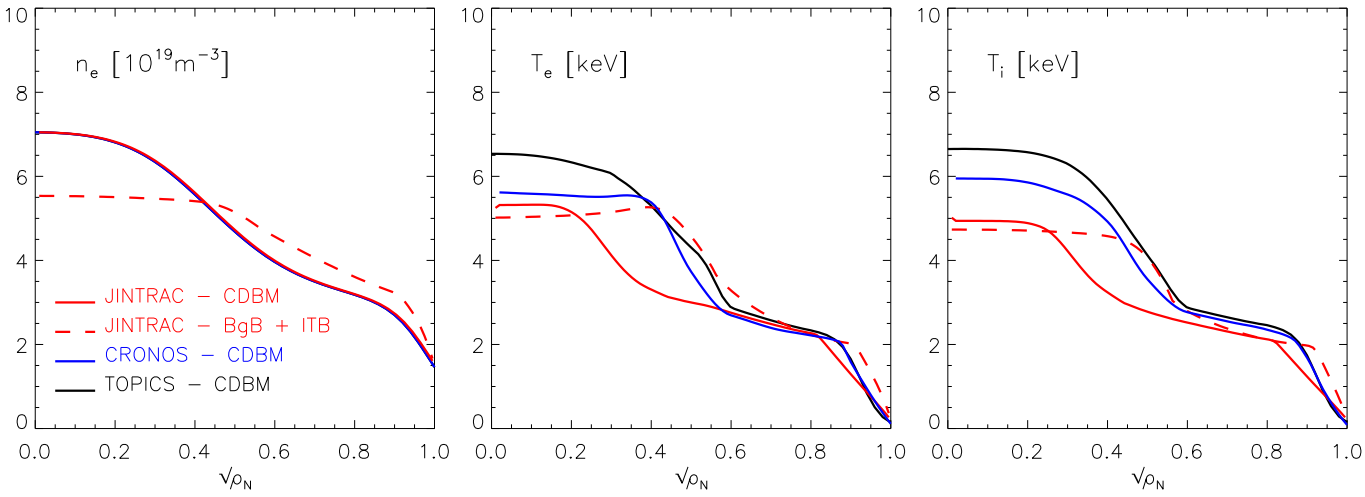

Figure 12. Predicted electron density, electron temperature and ion temperature profiles for a JT-60SA advanced steady-state plasma (scenario 5.1 'low power' version). The codes and the transport models used in the simulations are indicated in the legend.